

# Symmetry-constrained electron vortex propagation

L. Clark,<sup>1,\*</sup> G. Guzzinati,<sup>1</sup> A. Béch ,<sup>1</sup> A. Lubk,<sup>2</sup> and J. Verbeeck<sup>1</sup>

<sup>1</sup>EMAT, University of Antwerp, Groenenborgerlaan 171, 2020 Antwerp, Belgium

<sup>2</sup>Triebnberglabor, University of Dresden, Zum Triebnberg 1, 01062 Dresden, Germany

(Dated: March 3, 2016)

Electron vortex beams hold great promise for development in transmission electron microscopy, but have yet to be widely adopted. This is partly due to the complex set of interactions that occur between a beam carrying orbital angular momentum (OAM) and a sample. Herein, the system is simplified to focus on the interaction between geometrical symmetries, OAM and topology. We present multiple simulations, alongside experimental data to study the behaviour of a variety of electron vortex beams after interacting with apertures of different symmetries, and investigate the effect on their OAM and vortex structure, both in the far-field and under free-space propagation.

PACS numbers: 41.85.Ct, 42.79.Ag, 41.75.Fr, 42.30.Kq

## I. INTRODUCTION

Electron vortex beams, are electron states wherein the phase is structured to possess a phase singularity on axis, with a wave function of  $\Psi = A(r)e^{i\ell\phi}e^{ikz}$ . The amplitude function in this simple case, is a function of  $r$  alone. The paraxial beam propagates in the  $z$ -direction, with wave-number  $k$ . The value  $\ell$  is an integer, describing the topological charge, or winding number of the vortex. When the beam is in a simple, circularly symmetric state,  $\ell$  also determines the orbital angular momentum (OAM) of the beam [1].

Such electron beams were first considered explicitly in 2007 [2], having been alluded to previously [3, 4]. They were demonstrated experimentally in 2010 [5–7], and have remained under intense study since. The interest in these structured beams comes not only from a fundamental interest in their unusual behaviours [8–15], but also from prospects for novel applications in a variety of topics. Potential applications include magnetic chiral dichroism measurements [6, 16–18], being used to determine crystal chirality [19] and providing opportunities to use electron vortices as an analogue of optical tweezers [20].

The application most fervently awaited for electron vortex beams is that they may enable atomic-resolution electron magnetic circular dichroism (EMCD) [6, 16, 18], with better resolution than existing methods. While early experiments seemed encouraging, later studies revealed the complexity of the set-up, thus requiring further careful attention [21–23].

An electron beam interacts strongly with a sample [24], which rapidly changes the shape of the wavefront. For typical TEM sample thicknesses, multiple scattering is likely to occur, further complicating the interaction between the beam electron and the sample. If the beam is aligned with a crystal zone-axis of the sample, the interaction is particularly strong, and channelling will occur, biasing which parts of the sample are exposed to the probing electron [25]. This channelling will also affect the propagation of the vortex core [26, 27]. The local symmetry imposed on the beam by the crystal structure will also affect the OAM of the wave as it propagates [28]. All of these effects occur synchronously, leading to complicated details in the electron wave as it exits from the sample, and complex changes in any recorded electron energy-loss spectrograms (as these depend on the local electron wave-function).

Here, we aim to clarify one aspect of this complex system, by studying the effects of spatial confinement in a geometric symmetry on an electron vortex beam. This is loosely analogous to the effects of the crystal symmetry on the electron vortex beam, while avoiding the complexity of channelling, and other sample interaction effects.

Futhermore, in previous work we noted interesting behaviour of electron vortex beams, when microscope apertures are misaligned, or when using non-round apertures [26, 29, 30]. Particularly, following the interaction with apertures with discrete rotational-symmetries as in Guzzinati *et al.* [29], it can be seen that the original beam symmetry is not conserved, and a dark vortex core is not always found on axis. The interference between the aperture edge waves [31] and the vortex probe, leads to an intensity profile which reveals the topological charge of the input beam, in the case of a centred, single-ringed input vortex probe [32].

Such a non-circularly symmetric constraint prevents the beam from being in an OAM eigenstate, so a high-order vortex core may degenerate into an arrangement of multiple, displaced  $|\ell| = 1$  vortices [26]. We now deliberately apply these unusual settings to allow a deeper study of vortex splitting, propagation and reconnection.

---

\* Electronic address: laura.clark@uantwerp.be

We will investigate the vortex structure of an electron vortex beam after impinging on an aperture of a chosen geometry (round, square, equilateral triangle, off-centred circle), in the far-field, and during propagation. We will study this system both computationally and experimentally. Similar systems have been considered previously with optical vortex beams, but only with regard to the far-field behaviour of the beam. Here, we focus on the beam structure during propagation, as a route to a deeper understanding of electron vortices within a sample. In the following, we firstly compare the effects of the different geometric apertures on the far-field wave and vortex structures, comparing experimental data to our simulations. We then model the whole focal series of the beam, tracking the propagation of the vortex cores through the volume. We find a surprisingly complex vortex structure, which may be of significance to the development of the vortex-EMCD method.

## II. SYSTEM DESCRIPTION

Many different methods of producing electron vortex beams have been investigated. The first experimental electron vortex beam relied on an opportune stacking of graphite flakes [5]. This is not easily reproducible. After that, the holographic forked mask technique, borrowed from optics [33], was introduced [6], and developed further [7, 34–37]. Electron vortices produced through aberration manipulation were also investigated [38–41], as well as direct phase plate production [42, 43]. These methods however, all have their own foibles - primarily, limitations to the intensity in a given vortex order, or experimental limitations to the attainable purity of a given OAM state.

More recent developments however, have improved on this. It has been shown that illuminating the end of a long, thin, nanoscale bar magnet, can induce a vortex character into the electron beam, while only blocking a very small proportion of the incoming electron flux [44, 45]. Experimentally, if the magnetic needle is produced sufficiently accurately, the resultant vortex beam can have more than 95% of the beam’s intensity in the desired OAM state [46]. While this method results in the “best” electron vortex beams currently available, it is not well suited to investigating different orders of topological charge, as this would require access to a set of several magnetic needle apertures. To ensure the fairest comparison between a set of vortex beams of different order, we will thus investigate the beams resulting from a well-made forked holographic mask, ensuring they are sufficiently laterally separated. This has the benefit of having high OAM-mode purity, at the expense of lower beam intensity, not critical in the present study.

By using a forked holographic mask in the condenser plane of the microscope, we are able to produce a range of high-order vortex beams in the image plane, with diameters in the range of a few tens of nanometres (adjustable by tuning the condenser system). In the ideal, simple case, where the mask is designed by interfering a tilted plane wave with an  $\exp(i\ell\phi)$  term only (with no additional amplitude modulation), and the binarisation is applied at exactly half of the maximum intensity value, the bars in the resulting mask will be the same width as the gaps (as illustrated in figure 1a). In this case, the only beams produced will be the zero-order central beam (with  $\ell = 0$ ), and odd-ordered side beams (with  $|\ell| = 1, 3, 5, \dots$ ), due to the combination of diffraction envelopes creating missing orders [47].

However, in many experimental cases, this does not hold true, due to the challenges in the fine control of focused ion beam (FIB) milling time [35], leading to other vortex orders appearing, at varying intensities. The milling of our present experimental mask enables access to  $|\ell| = (0, 1, 2, 3)$  vortex orders with reasonable intensities.

For maximum diffractive effects, we want to produce the geometric apertures such that they are of a similar size to the vortex beams at the sample plane. Producing apertures at this scale is challenging; we make use of the conjugated selected area plane instead. There is a demagnification factor of approximately 70 between the selected area plane in our microscope, and the image plane, allowing us to use apertures with a characteristic dimension of  $2\mu\text{m}$ . This is projected to the image plane as a characteristic dimension of 30 nm, a similar size to the vortex beams we produce from a forked mask with diameter  $10\mu\text{m}$  (approximately 0.25 mrad) when slightly defocused to optimally fill the apertures.

In this way, we can illuminate each of the geometric apertures with electron-vortex beams of different topological charges. We can image the far-field diffraction of each, and compare with simulations to investigate the resulting vortex structure. Furthermore, we can also manipulate the diffraction and projector lenses, such as to image a full series of the electron-vortex propagation volume, allowing us to study the free-space propagation of a pure vortex state after passing through a specific aperture. This will show how a pure state splits into a complicated combination of vortex states, depending on the symmetry of the system.

### A. Distinguishing topological charge, and orbital angular momentum

OAM and topological charge are often used interchangeably. They do coincide in the well-studied case of a single, on-axis vortex beam. However, in the general case, they are different [48]. They can differ in magnitude even in some

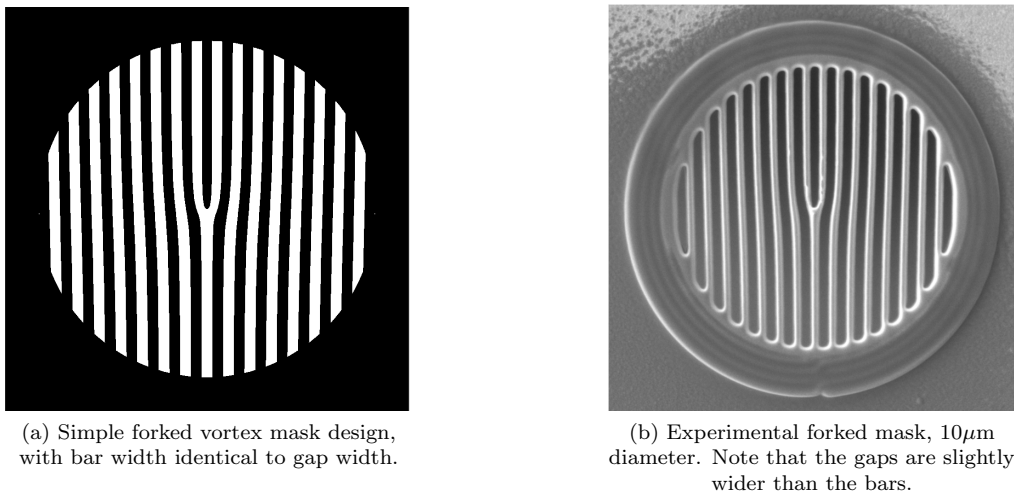


FIG. I. Theoretical and experimental comparison of forked mask apertures.

on-axis, circularly symmetric cases [49], or differ in both sign and magnitude [50]. To aid clarity in the following sections, we explicitly define these concepts here.

Topological charge is identical to winding number and is a local property. It describes the number of times the phase passes through  $2\pi$  around a closed loop,  $C$  :

$$\ell = \frac{1}{2\pi} \oint_C d\phi \quad (1)$$

If the loop itself passes through no zero intensity points,  $\ell$  is constrained to being an integer. The total topological charge in a region is only affected by the discrete points of phase discontinuity within that region. For an in depth discussion on the nature of topological charge, see the work of Dennis [51].

OAM is axis-dependent, varying strongly with where in the beam it is measured from. It is only conserved in a circularly symmetric system [52]. Typically, in our paraxial systems, we are only interested in the  $z$ -component of the expectation value of the OAM:

$$\langle L_z \rangle = \langle \Psi | \hat{L}_z | \Psi \rangle \quad (2)$$

where, in cylindrical coordinates,  $\hat{L}_z = -i\hbar \frac{\partial}{\partial \theta}$  [28, 53]. In a system with discrete, rotational symmetry, a pure input state will broaden into a superposition of OAM modes upon propagation. The input vortex core may degenerate into a beam with multiple first-order vortices, displaced from the centre of the incoming beam. Pairs of  $+1, -1$  vortices can also be created, or annihilated within a freely propagating system, forming 3D vortex loops which do not change the global topology of the system [26, 54].

### B. Endurance of geometrical symmetry

In addition to the propagation behaviour enforced by the conservation of topology, the standard behaviour of Fourier optics must still apply. It is trivial to show that the intensity pattern in the far-field of a plane wave limited by an aperture, is the squared modulus of the Fourier transform of the wave in the aperture plane [55]. Distorting the input wave from a planar wave-front to something else will lead to a convolution of the Fourier transform of the aperture shape, with the Fourier transform of the input wave. Combining these effects means that the complete rotational symmetry of the incoming vortex beam is reduced to the discrete rotational symmetry of the aperture.

## III. FAR-FIELD BEHAVIOUR

We begin investigating these effects, by studying far-field intensities of different vortex beam orders on a set of apertures, with different rotational symmetries.

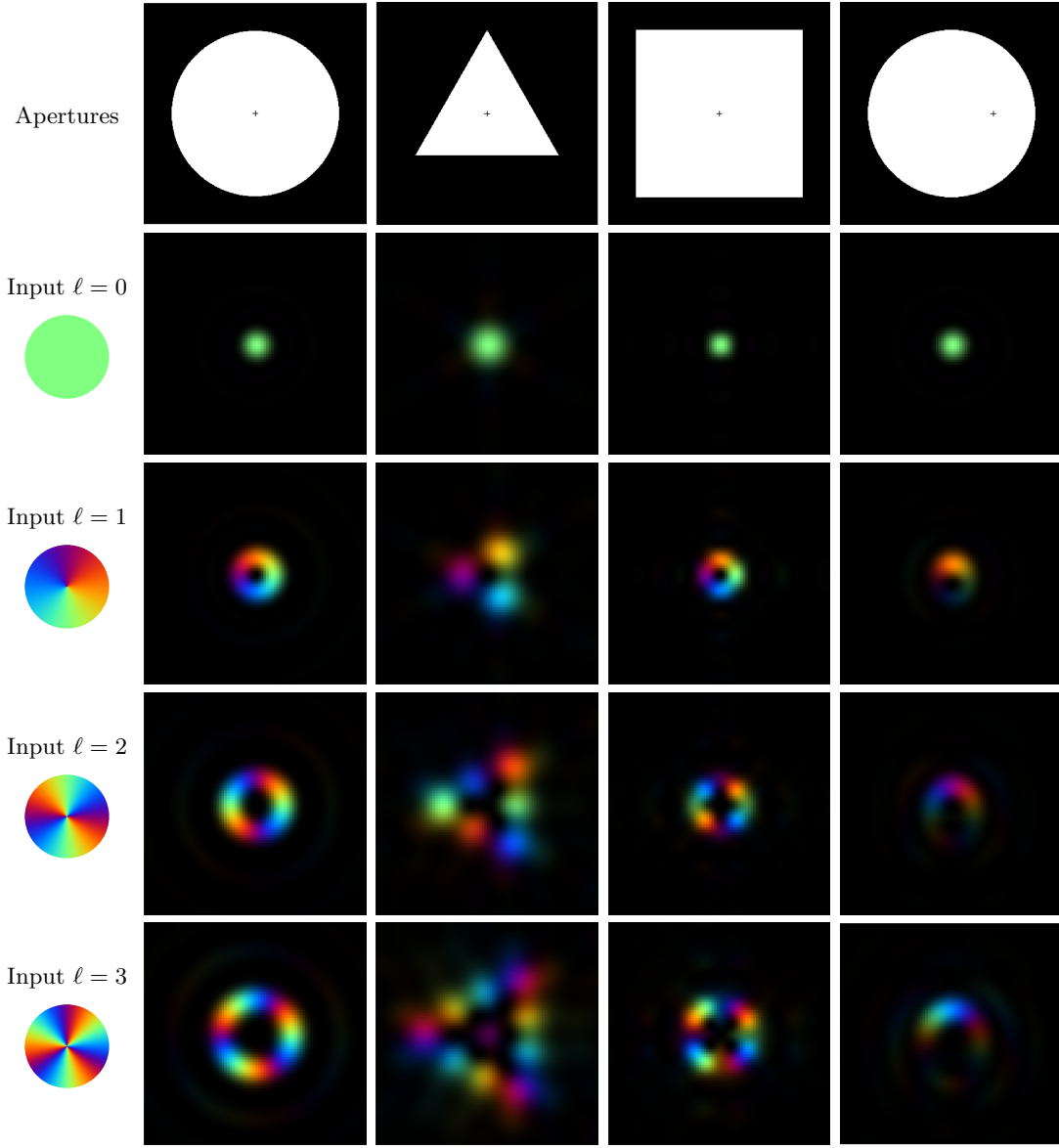


FIG. II. Simulated apertures and far-field intensity patterns resulting from the vortex beams of different order. The  $0-2\pi$  phase colour map is illustrated in the  $\ell = 1$  incoming vortex probe. The  $+$  markers in the apertures highlight the centre of the incoming vortex beam. The apertures have edge lengths, or diameters of  $2\mu\text{m}$ .

### A. Simulated Results

Firstly, the far-field results of illuminating a series of geometrical apertures were simulated. The chosen apertures were a centred circle, an equilateral triangle, a square, and a circle displaced by half a radius. In Fig. II, these apertures are illustrated, along with figures representing the intensity (brightness) and phase (hue) of the wave in the far-field of the aperture, when illuminated with the vortex beams of different order. The vortex beam was modelled as a beam resulting from the far-field diffraction of a forked holographic mask, with the size chosen such that the peak intensity ring of the vortex approximately matched the size of the aperture.

### B. Experimental Results

The corresponding experiments were then performed in an aberration-corrected FEI Titan<sup>3</sup> microscope operating at 200 keV, resulting in the data illustrated in Fig. III. The forked aperture was located in the condenser plane and

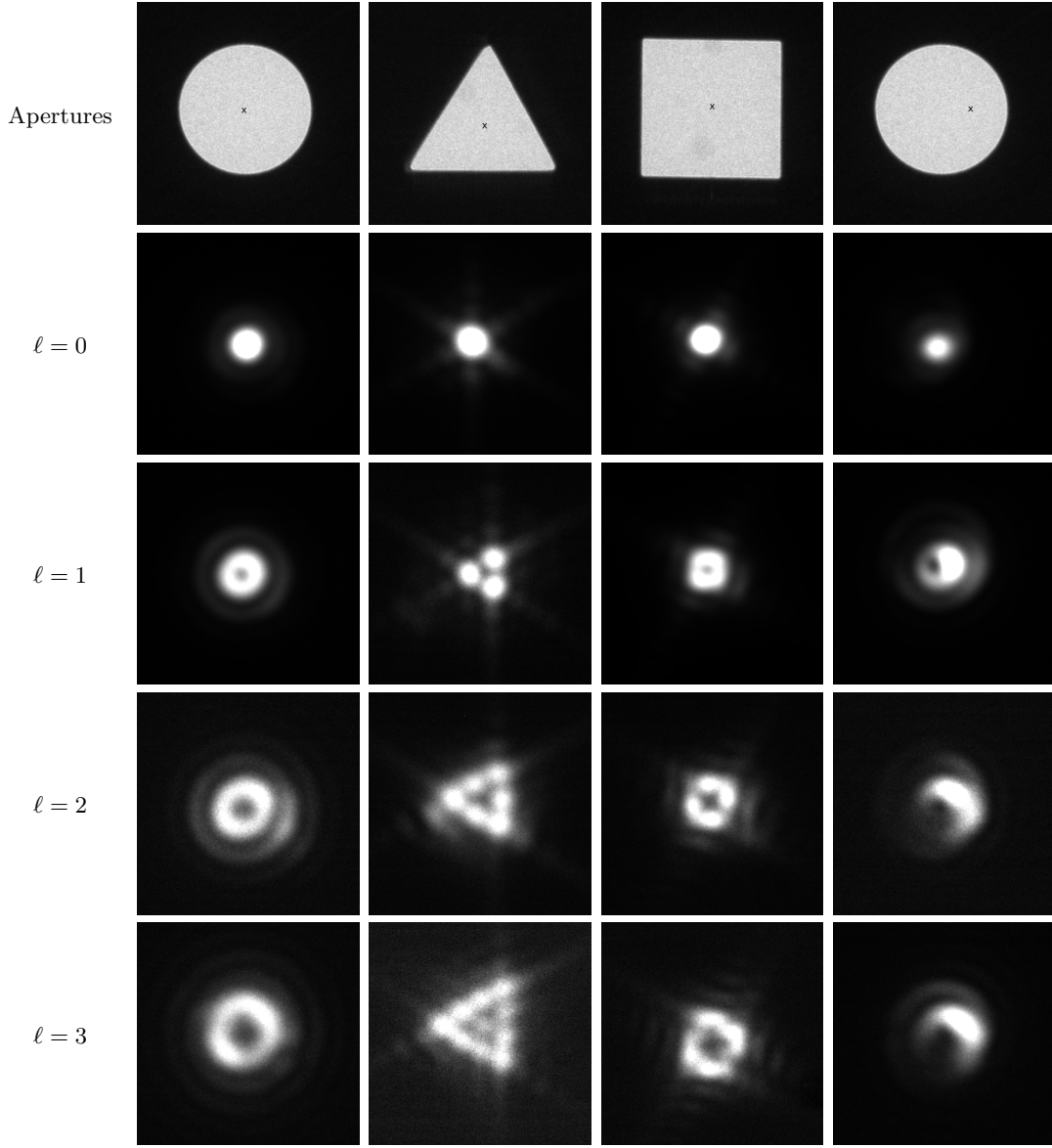


FIG. III. Experimental apertures and far-field intensity patterns resulting from vortex beams of different order. The  $X$  markers in the apertures highlight the centre of the incoming vortex beam. The apertures have edge lengths, or diameters of  $2\,\mu\text{m}$ .

the geometric apertures were in the selected-area plane.

Comparing the simulated and experimental far-field images, as shown in Fig. II and Fig. III, we can see a very good agreement in the intensity profiles. The results begin to diverge in the  $\ell = 3$  data set, as these beams pass at a higher angle to the optical axis through the microscope from the forked mask and thus are more sensitive to the residual aberrations.

The trivial  $\ell = 0$  cases simply show the intensity of a Fourier-transformed approximately-Gaussian beam, apodized by these apertures [47]. The  $\ell = 0$  triangle case begins to reveal the discrete symmetry. Friedel's law points out that the Fourier transform of a real function is centrosymmetric, and thus the intensity pattern of diffraction from a triangular aperture will have six-fold symmetry. However, when the conditions for Friedel's law are broken, such as by a non-real, or phase-structured incoming wave (such as in the  $|\ell| \geq 1$  cases), the diffraction pattern is no longer compelled to be centrosymmetric [19], and the diffraction pattern can then reveal more directional information about the probe. For example, Mourka *et al.* established that diffraction of an optical vortex beam from an aperture without  $180^\circ$  rotational symmetry can determine its handedness, through interaction of the OAM-induced rotation, with the Gouy phase [56, 57]. It has also been shown, in both light optics and electron microscopy, that diffraction of a single-ringed vortex beam from a triangular aperture enables a quantification of the topological order of the vortex

beam, by counting the  $|\ell| + 1$  intensity lobes found along one edge of the resultant triangular pattern of lobes [29, 32]. A closer look at the intensity profile of the  $\ell = 3$  triangle case in figure III, reveals a faint intensity lobe on-axis, even in the idealised simulation in figure II. This is unusual in coherent vortex studies, and warrants further attention. A related unusual effect can be seen in the  $\ell = 3$  square case, where in the centre of the intensity profile, five dark spots can be seen, arranged as on a die.

To investigate the cause of these effects, the simulations were further developed to highlight the vortex cores and determine their handedness. In a small, pixellated loop around a vortex core, phase aliasing errors can quickly creep in when dealing with higher order vortices (with their rapid phase changes). To avoid this complication, images shown in figure IV only differentiate between the left- or right- handedness of the vortices, and not their topological order.

In the first column of figure IV, we see the standard behaviour of the unperturbed beam, the single vortex core of each beam remains stable and on-axis, as the cylindrical symmetry permits OAM-eigenstates [58]. There are phase jumps of  $\pi$  between each ring in the tails of the Airy disc, but these do not affect the vortex behaviour in this cylindrically-symmetric case.

However, in the triangle and square cases (second and third columns of figure IV) vortices are abundantly present in the  $\ell = 0$  far-field profiles. This is due to the interference between the different sets of Fresnel fringes propagating from the aperture sides [31] in such a way as to produce arrays of  $(+1, -1)$  vortices, similarly to the vortex lattices produced by Niermann *et al.* [59].

In addition to the many vortex-antivortex pairs created in the outer region of the pattern, in some of the higher order cases, we can also note interesting splitting behaviours of the central vortex. The splitting only occurs when the order of the vortex is greater than half of the order of the rotational symmetry of the aperture - this inequality was first noted by Ferrando [52]. We see evidence of this in the  $\ell = 2$ , square aperture case. It is unusual for a high order vortex not to degenerate in a non-circularly symmetric system, but as in this case,  $|m| \leq \frac{n}{2}$ , following the notation of García-March *et al.*, where integer  $m$  is the angular momentum of the input beam, and  $n$  is the order of rotational symmetry of the system [60]. In the case where the vortex order matches the geometrical, rotational symmetry of the aperture, such as in the  $\ell = 3$  beam in a triangle, we see the vortex splits into  $\ell$  distinct vortices of order one. In cases where the vortex order does not match the aperture symmetry, but does surpass Ferrando's inequality, such that the vortex core must degenerate, additional  $(+1, -1)$  vortex pairs can be created such that both topological and geometrical requirements are fulfilled. This effect we see clearly in the  $\ell = 2$  triangle case, and the  $\ell = 3$  square case where in the central region of the diffraction pattern, we can see extra vortex cores in figure IV. The off-centred circle however, shows a rather different vortex structure, due to the complete absence of rotational symmetry in the system. In this case, the higher-order vortices split without creation of additional vortices in the central region of the diffraction pattern. There are many  $(+1, -1)$  vortex pairs in the surrounding area, and particularly along a line perpendicular to the aperture-shift direction (half of the Gouy rotation for a full image-to-image propagation [61]). The rotations seen in the experimental case do not match this, due to the experimental difficulties in positioning the aperture. We note the interesting parallel between this infinite line of vortices, and the vortices resulting from a fractional phase step [62].

### C. Propagation series

The far-field structures certainly have interesting and unusual structures, which are structurally very different from the input wave-fronts. For this reason, we decided to also investigate the wave-front structure upon propagation.

A simulation was built around a thin-lens model, propagating from the image plane (showing the aperture outline) towards the back-focal plane (containing the far-field image). This range is too large to be numerically modelled with a simple Fresnel propagator, without encountering the sampling issues common in such propagation methods [63]. A modified linear canonical transform (LCT) algorithm was used instead, wherein the fractional Fourier transform allows us to sample the full range of the propagation volume. The modelled system is an  $\ell = 3$  Laguerre-Gaussian vortex beam, illuminating a square aperture. This example was selected as it displays most of the interesting features in one system.

Experimentally, this was performed at 300 keV, with the same microscope set-up as described in section III B. The focal series is obtained by defocussing from the far-field intensity pattern, towards an image of the aperture. This defocussing however, changes the currents in the diffraction lens, such that the principal planes, and relative position become undefined. Subsequently, the magnification of the system changes non-linearly with the defocus. For this reason, the experimental focal series data are unscaled, and can only be compared qualitatively with the simulations. Accordingly, the simulations are unscaled in the  $(x, y)$  plane.

The simulation and experiment match closely, as can be seen in sample images from each focal series, displayed in Fig. V. From the simulated series, we are also able to locate the vortex cores (using the same algorithm as for Fig. IV), in each  $(x, y)$  plane. These can then be collated over the series in  $z$  by tracking isosurfaces enclosing volumes of

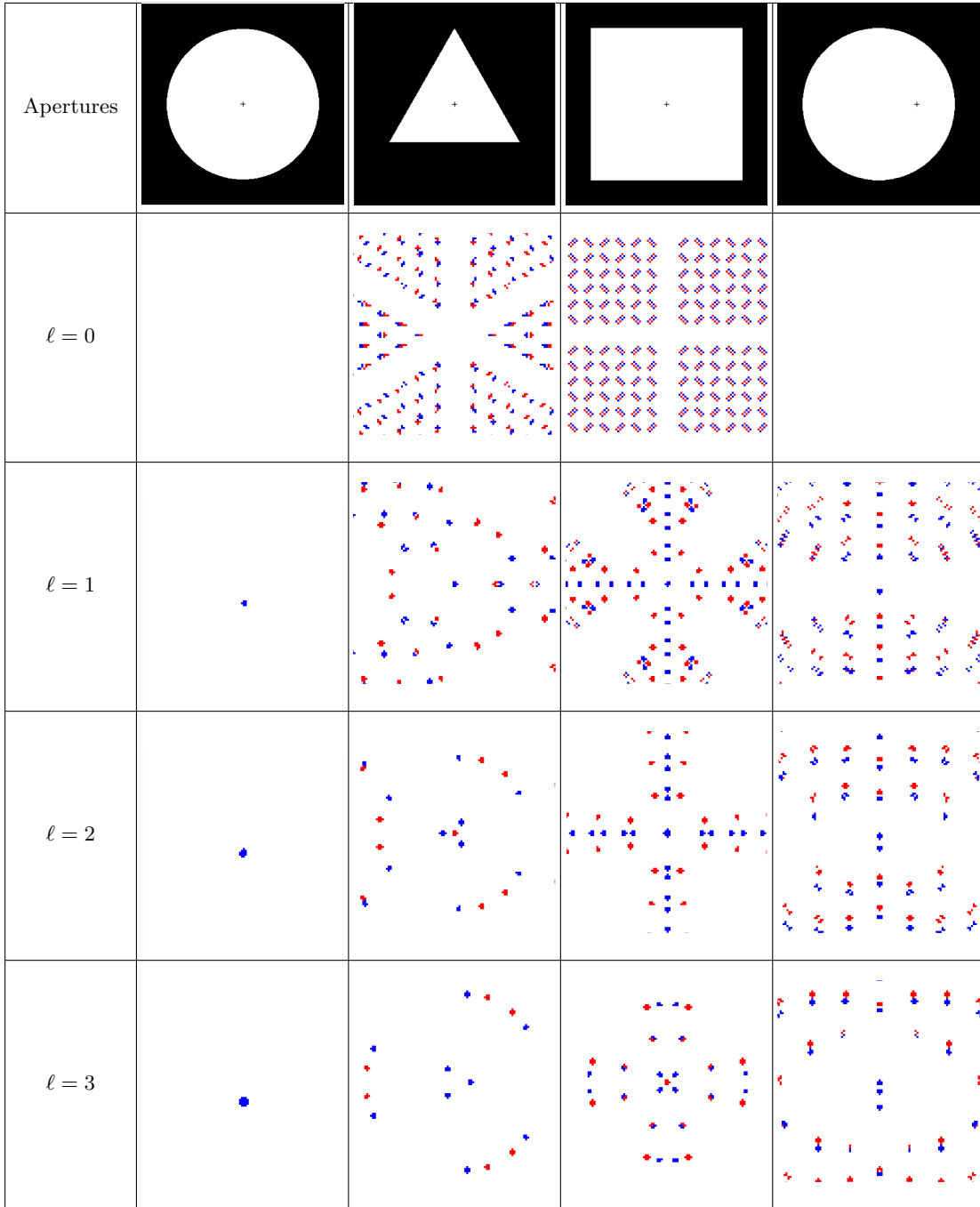


FIG. IV. Simulated apertures and far-field vortex patterns resulting from the vortex beams of different order. The + markers in the apertures highlight the centre of the incoming vortex beam. Blue corresponds to a positive (right-handed) vortex core, while red corresponds to a negative (left-handed) vortex core.

high vorticity. This is shown in figure VI.

In this figure, we can see several different regimes, as highlighted by the annotations. The incoming single vortex at the bottom of the figure is initially stable. The vortex core then splits into a complex lattice of vortices - the requirement of at least three-plane wave interference for a vortex lattice are met, with edge waves meeting the paraxial beam [64], leading to the initial vortex bifurcations. Looking further from the aperture in  $z$ , the created vortices annihilate in  $(+1, -1)$  pairs. This is possible due to the presence of more than three plane waves [65]. The system cannot be expressed in only a few plane wave terms, and hence the output is very complex. The periodicity of the vortex creation-annihilation loops decreases, with the frequency of the Fresnel fringes under propagation, until

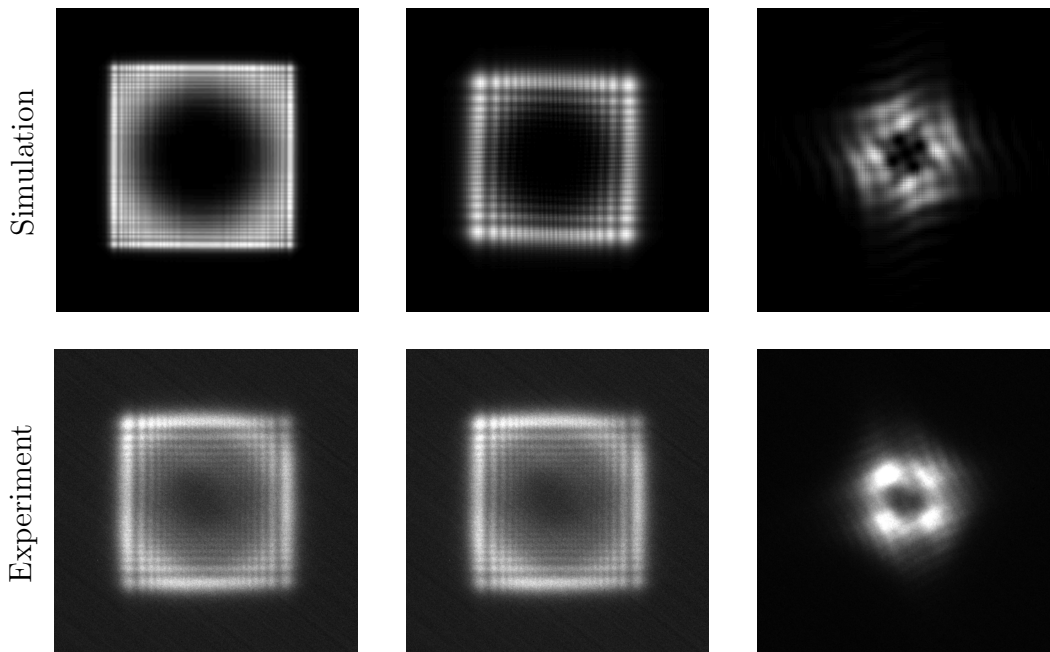


FIG. V. Propagation series of an  $\ell = 3$  vortex beam after a square aperture, from near-field (left), towards the far-field (right). The upper row shows simulated data (perfect coherence); the lower row shows experimental data.

the far-field is reached, transitioning approximately as the Fresnel number approaches  $F = 1$ .

As the system reaches the far-field, the rules defined by Ferrando and García-March express themselves more clearly [66], with the  $\langle \ell \rangle = 3$  form of the beam in a square symmetry, composed of four  $\ell = +1$ , and one  $\ell = -1$  vortex cores in the central region. In this diffraction pattern, around 86% of the wavefront is found to still be in an  $\ell = 3$  state (measured over the whole wave, on-axis, using the decomposition method employed in Ref. [39]).

Unlike the model system of O'Holloran *et al.*, we do not see any interlinked, closed loops [67]. This is probably due to the predominant  $z$ -only momentum of the system. Unlike Dennis *et al.* we do not see any knots (excluding the unknot) [68], due to the non-generic aperture shapes required to produce a knot.

#### IV. CONCLUSION

We have studied the propagation of vortex cores in electron vortex beams in non-rotationally symmetric systems. High-order vortex cores were shown to split, and it is demonstrated that a stable far-field pattern, can include more vortex-antivortex pairs than were present in the initial condition. The propagation volume leading to such patterns was investigated for the first time, and its complexity was studied. The vortex structure under near-field conditions was found to be exceptionally detailed.

The instability of vortices, and the ease with which they can be created under propagation, are significant contributing factors to the challenges in utilising electron vortex beams to reproducibly measure magnetic states of a material using electron energy-loss spectroscopy (EELS). The results presented in this paper suggest that to optimise vortex-EMCD, the effect of the lattice symmetry on the vortex beam needs to be minimised, perhaps through careful selection of beam convergence angle, and channelling conditions.



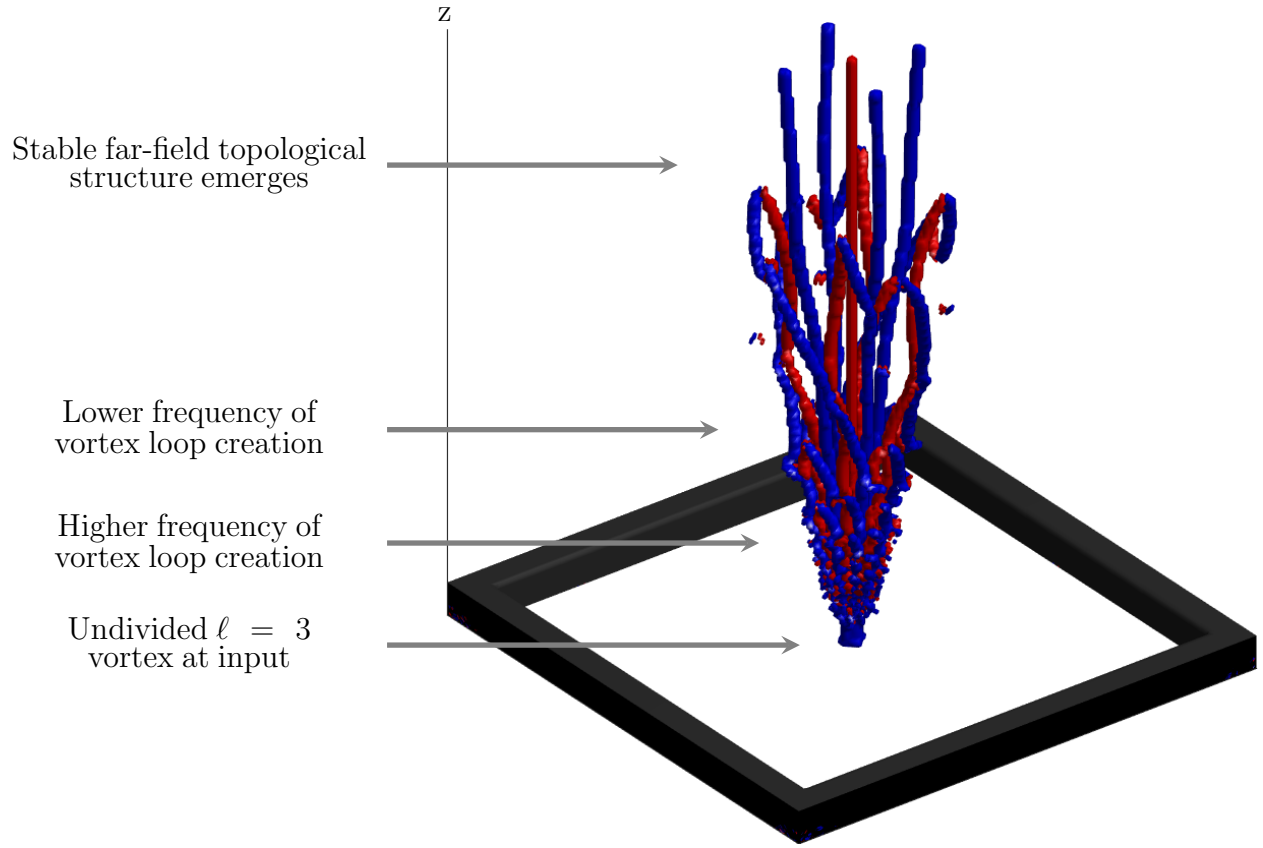


FIG. VI. Tracking of the vortex cores of an  $\ell = 3$  vortex core, illuminating a square aperture to the far-field. Blue corresponds to a positive (right-handed) vortex core, while red corresponds to a negative (left-handed) vortex core.

## V. REFERENCES

- 
- [1] Les Allen, Marco W Beijersbergen, RJC Spreeuw, and JP Woerdman, “Orbital angular momentum of light and the transformation of laguerre-gaussian laser modes,” *Physical Review A* **45**, 8185 (1992).
  - [2] Konstantin Yu Bliokh, Yury P Bliokh, Sergey Savel’ev, and Franco Nori, “Semiclassical dynamics of electron wave packet states with phase vortices,” *Physical review letters* **99**, 190404 (2007).
  - [3] Iwo Bialynicki-Birula, Zofia Bialynicka-Birula, and Cezary Śliwa, “Motion of vortex lines in quantum mechanics,” *Physical Review A* **61**, 032110 (2000).
  - [4] Akira Fukuhara, Kohsei Shinagawa, Akira Tonomura, and Hideo Fujiwara, “Electron holography and magnetic specimens,” *Physical Review B* **27**, 1839 (1983).
  - [5] Masaya Uchida and Akira Tonomura, “Generation of electron beams carrying orbital angular momentum,” *Nature* **464**, 737–739 (2010).
  - [6] Johan Verbeeck, He Tian, and Peter Schattschneider, “Production and application of electron vortex beams,” *Nature* **467**, 301–304 (2010).
  - [7] Benjamin J McMorran, Amit Agrawal, Ian M Anderson, Andrew A Herzing, Henri J Lezec, Jabez J McClelland, and John Unguris, “Electron vortex beams with high quanta of orbital angular momentum,” *Science* **331**, 192–195 (2011).
  - [8] Ruben Van Boxem, Jo Verbeeck, and Bart Partoens, “Spin effects in electron vortex states,” *EPL (Europhysics Letters)* **102**, 40010 (2013).
  - [9] Ruben Van Boxem, Bart Partoens, and Johan Verbeeck, “Rutherford scattering of electron vortices,” *Physical Review A* **89**, 032715 (2014).
  - [10] Ruben Van Boxem, Bart Partoens, and Jo Verbeeck, “Inelastic electron-vortex-beam scattering,” *Phys. Rev. A* **91**, 032703 (2015).
  - [11] Sophia Marriott Lloyd, Mohamed Babiker, and Jun Yuan, “Interaction of electron vortices and optical vortices with

- matter and processes of orbital angular momentum exchange,” *Physical Review A* **86**, 023816 (2012).
- [12] SM Lloyd, M Babiker, J Yuan, and C Kerr-Edwards, “Electromagnetic vortex fields, spin, and spin-orbit interactions in electron vortices,” *Physical review letters* **109**, 254801 (2012).
  - [13] Konstantin Y Bliokh, Mark R Dennis, and Franco Nori, “Relativistic electron vortex beams: angular momentum and spin-orbit interaction,” *Physical review letters* **107**, 174802 (2011).
  - [14] BG Mendis, “Dynamic scattering of electron vortex beams—a bloch wave analysis,” *Ultramicroscopy* **149**, 74–85 (2015).
  - [15] Yuya Hasegawa, Koh Saitoh, Nobuo Tanaka, Shogo Tanimura, and Masaya Uchida, “Young’s interference experiment with electron beams carrying orbital angular momentum,” *Journal of the Physical Society of Japan* **82**, 033002 (2013).
  - [16] Peter Schattschneider, Stefan Löffler, Michael Stöger-Pollach, and Johan Verbeeck, “Is magnetic chiral dichroism feasible with electron vortices?” *Ultramicroscopy* **136**, 81–85 (2014).
  - [17] Johan Verbeeck, Peter Schattschneider, Sorin Lazar, Michael Stöger-Pollach, Stefan Löffler, Andreas Steiger-Thirsfeld, and Gustaaf Van Tendeloo, “Atomic scale electron vortices for nanoresearch,” *Applied Physics Letters* **99**, 203109 (2011).
  - [18] Ján Rusz and Somnath Bhowmick, “Boundaries for efficient use of electron vortex beams to measure magnetic properties,” *Physical review letters* **111**, 105504 (2013).
  - [19] Roeland Juchtmans, Armand Béch , Artem Abakumov, Maria Batuk, and Jo Verbeeck, “Using electron vortex beams to determine chirality of crystals in transmission electron microscopy,” *Physical Review B* **91**, 094112 (2015).
  - [20] Jo Verbeeck, He Tian, and Gustaaf Van Tendeloo, “How to manipulate nanoparticles with an electron beam?” *Advanced materials* **25**, 1114–1117 (2013).
  - [21] Ján Rusz, Somnath Bhowmick, Mattias Eriksson, and Nikolaj Karlsson, “Scattering of electron vortex beams on a magnetic crystal: Towards atomic-resolution magnetic measurements,” *Physical Review B* **89**, 134428 (2014).
  - [22] Ján Rusz, Juan-Carlos Idrobo, and Somnath Bhowmick, “Achieving atomic resolution magnetic dichroism by controlling the phase symmetry of an electron probe,” *Physical review letters* **113**, 145501 (2014).
  - [23] Darius Pohl, Sebastian Schneider, Jan Rusz, and Bernd Rellinghaus, “Electron vortex beams prepared by a spiral aperture with the goal to measure EMCd on ferromagnetic films via stem,” *Ultramicroscopy* **150**, 16–22 (2015).
  - [24] Richard Henderson, “The potential and limitations of neutrons, electrons and x-rays for atomic resolution microscopy of unstained biological molecules,” *Quarterly reviews of biophysics* **28**, 171–193 (1995).
  - [25] NR Lugg, G Kothleitner, N Shibata, and Y Ikuhara, “On the quantitiveness of EDS STEM,” *Ultramicroscopy* **151**, 150–159 (2015).
  - [26] Axel Lubk, Laura Clark, Giulio Guzzinati, and Jo Verbeeck, “Topological analysis of paraxially scattered electron vortex beams,” *Physical Review A* **87**, 033834 (2013).
  - [27] Stefan Löffler and Peter Schattschneider, “Elastic propagation of fast electron vortices through crystals,” *Acta Crystallographica Section A: Foundations of Crystallography* **68**, 443–447 (2012).
  - [28] Gabriel Molina-Terriza, Juan P Torres, and Lluís Torner, “Management of the angular momentum of light: preparation of photons in multidimensional vector states of angular momentum,” *Physical review letters* **88**, 013601 (2001).
  - [29] Giulio Guzzinati, Laura Clark, Armand Béch , and Jo Verbeeck, “Measuring the orbital angular momentum of electron beams,” *Physical Review A* **89**, 025803 (2014).
  - [30] L Clark, A Béch , G Guzzinati, and J Verbeeck, “Quantitative measurement of orbital angular momentum in electron microscopy,” *Physical Review A* **89**, 053818 (2014).
  - [31] Joseph B Keller, “Geometrical theory of diffraction,” *JOSA* **52**, 116–130 (1962).
  - [32] JM Hickmann, EJS Fonseca, WC Soares, and S Ch vez-Cerda, “Unveiling a truncated optical lattice associated with a triangular aperture using light’s orbital angular momentum,” *Physical review letters* **105**, 053904 (2010).
  - [33] V Yu Bazhenov, MV Vasnetsov, and MS Soskin, “Laser beams with screw dislocations in their wavefronts,” *JETP Letters* **52**, 429–431 (1990).
  - [34] Jo Verbeeck, He Tian, and Armand Béch , “A new way of producing electron vortex probes for stem,” *Ultramicroscopy* **113**, 83–87 (2012).
  - [35] Laura Clark, *Electron vortex beams: production and propagation*, Master’s thesis, University of York (2012).
  - [36] Vincenzo Grillo, Gian Carlo Gazzadi, Ebrahim Karimi, Erfan Mafakheri, Robert W Boyd, and Stefano Frabboni, “Highly efficient electron vortex beams generated by nanofabricated phase holograms,” *Applied Physics Letters* **104**, 043109 (2014).
  - [37] Tyler R Harvey, Jordan S Pierce, Amit K Agrawal, Peter Ercius, Martin Linck, and Benjamin J McMorran, “Efficient diffractive phase optics for electrons,” *New Journal of Physics* **16**, 093039 (2014).
  - [38] TC Petersen, Matthew Weyland, DM Paganin, TP Simula, SA Eastwood, and MJ Morgan, “Electron vortex production and control using aberration induced diffraction catastrophes,” *Physical review letters* **110**, 033901 (2013).
  - [39] L Clark, A Béch , G Guzzinati, A Lubk, M Mazilu, R Van Boxem, and J Verbeeck, “Exploiting lens aberrations to create electron-vortex beams,” *Physical review letters* **111**, 064801 (2013).
  - [40] Peter Schattschneider, Michael St ger-Pollach, and Johan Verbeeck, “Novel vortex generator and mode converter for electron beams,” *Physical review letters* **109**, 084801 (2012).
  - [41] Amir H Tavabi, Vadim Migunov, Christian Dwyer, Rafal E Dunin-Borkowski, and Giulio Pozzi, “Tunable caustic phenomena in electron wavefields,” *Ultramicroscopy* (2015).
  - [42] Roy Shiloh, Yossi Lereah, Yigal Lilach, and Ady Arie, “Sculpturing the electron wave function using nanoscale phase masks,” *Ultramicroscopy* **144**, 26–31 (2014).
  - [43] A B ch , R Winkler, H Plank, F Hofer, and J Verbeeck, “Focused electron beam induced deposition as a tool to create electron vortices,” *Micron* **80**, 34–38 (2016).
  - [44] Armand B ch , Ruben Van Boxem, Gustaaf Van Tendeloo, and Jo Verbeeck, “Magnetic monopole field exposed by electrons,” *Nature Physics* **10**, 26–29 (2014).

- [45] AM Blackburn and JC Loudon, “Vortex beam production and contrast enhancement from a magnetic spiral phase plate,” *Ultramicroscopy* **136**, 127–143 (2014).
- [46] Armand B  ch   and Jo Verbeeck, “Efficient creation of electron vortex beams for high resolution stem imaging,” *Ultramicroscopy* **To be published** (2016).
- [47] Eugene Hecht, *Optics* (Addison Wesley, 1998).
- [48] MV Berry, “Optical currents,” *Journal of Optics A: Pure and Applied Optics* **11**, 094001 (2009).
- [49] Anderson M Amaral, Edilson L Falc  o-Filho, and Cid B de Ara  jo, “Characterization of topological charge and orbital angular momentum of shaped optical vortices,” *Optics express* **22**, 30315–30324 (2014).
- [50] G. Molina-Terriza, “Vortex transformations and vortex dynamics in optical fields,” in *The angular momentum of light*, edited by David L Andrews and Mohamed Babiker (Cambridge University Press, 2012) pp. 31–50.
- [51] Mark Richard Dennis, *Topological singularities in wave fields*, Ph.D. thesis, University of Bristol (2001).
- [52] Albert Ferrando, “Discrete-symmetry vortices as angular bloch modes,” *Physical Review E* **72**, 036612 (2005).
- [53] P Schattschneider and J Verbeeck, “Theory of free electron vortices,” *Ultramicroscopy* **111**, 1461–1468 (2011).
- [54] LJ Allen, HML Faulkner, MP Oxley, and David Paganin, “Phase retrieval and aberration correction in the presence of vortices in high-resolution transmission electron microscopy,” *Ultramicroscopy* **88**, 85–97 (2001).
- [55] Joseph W Goodman, *Introduction to Fourier optics* (Roberts and Company Publishers, 2005).
- [56] A Mourka, J Baumgartl, C Shanor, K Dholakia, and EM Wright, “Visualization of the birth of an optical vortex using diffraction from a triangular aperture,” *Optics express* **19**, 5760–5771 (2011).
- [57] Areti Mourka, *Probing the modal characteristics of novel beam shapes*, Ph.D. thesis, University of St Andrews (2014).
- [58] David L Andrews and Mohamed Babiker, *The angular momentum of light* (Cambridge University Press, 2012).
- [59] T Niermann, J Verbeeck, and M Lehmann, “Creating arrays of electron vortices,” *Ultramicroscopy* **136**, 165–170 (2014).
- [60] M-   Garc  a-March, A Ferrando, Mario Zacar  s, J Vijande, and Lincoln D Carr, “Angular pseudomomentum theory for the generalized nonlinear schr  dinger equation in discrete rotational symmetry media,” *Physica D: Nonlinear Phenomena* **238**, 1432–1438 (2009).
- [61] Giulio Guzzinati, Peter Schattschneider, Konstantin Y Bliokh, Franco Nori, and Jo Verbeeck, “Observation of the Larmor and Gouy rotations with electron vortex beams,” *Physical review letters* **110**, 093601 (2013).
- [62] MV Berry, “Optical vortices evolving from helicoidal integer and fractional phase steps,” *Journal of Optics A: Pure and Applied Optics* **6**, 259 (2004).
- [63] John J Healy and John T Sheridan, “Sampling and discretization of the linear canonical transform,” *Signal Processing* **89**, 641–648 (2009).
- [64] Jan Masajada and Bogus  awa Dubik, “Optical vortex generation by three plane wave interference,” *Optics Communications* **198**, 21–27 (2001).
- [65] Kevin O’Holleran, Miles J Padgett, and Mark R Dennis, “Topology of optical vortex lines formed by the interference of three, four, and five plane waves,” *Optics Express* **14**, 3039–3044 (2006).
- [66] A Ferrando and MA Garc  a-March, “Theory for the control of dark rays by means of discrete symmetry diffractive elements,” *Journal of Optics* **15**, 044014 (2013).
- [67] Kevin O’Holleran, Mark R Dennis, and Miles J Padgett, “Topology of light’s darkness,” *Physical review letters* **102**, 143902 (2009).
- [68] Mark R Dennis, Robert P King, Barry Jack, Kevin O’Holleran, and Miles J Padgett, “Isolated optical vortex knots,” *Nature Physics* **6**, 118–121 (2010).

## ACKNOWLEDGMENTS

L.C., A.B., G.G, and J.V. acknowledge funding from the European Research Council under the 7th Framework Program (FP7), ERC Starting Grant No. 278510 - VORTEX. J.V. and A.L. acknowledge financial support from the European Union under the 7th Framework Program (FP7) under a contract for an Integrated Infrastructure Initiative (Reference No. 312483 ESTEEM2). The Qu-Ant-EM microscope was partly funded by the Hercules fund from the Flemish Government.